Electronic Supplementary Material (ESI) for Nanoscale.

Supporting Information

Cobalt vanadium chalcogenide microspheres decorated with dendrite-like fiber nanostructure for flexible wire-typed energy conversion and storage microdevices

Leila Naderi, Saeed Shahrokhian*

Department of Chemistry, Sharif University of Technology, Tehran 11155−9516, Iran

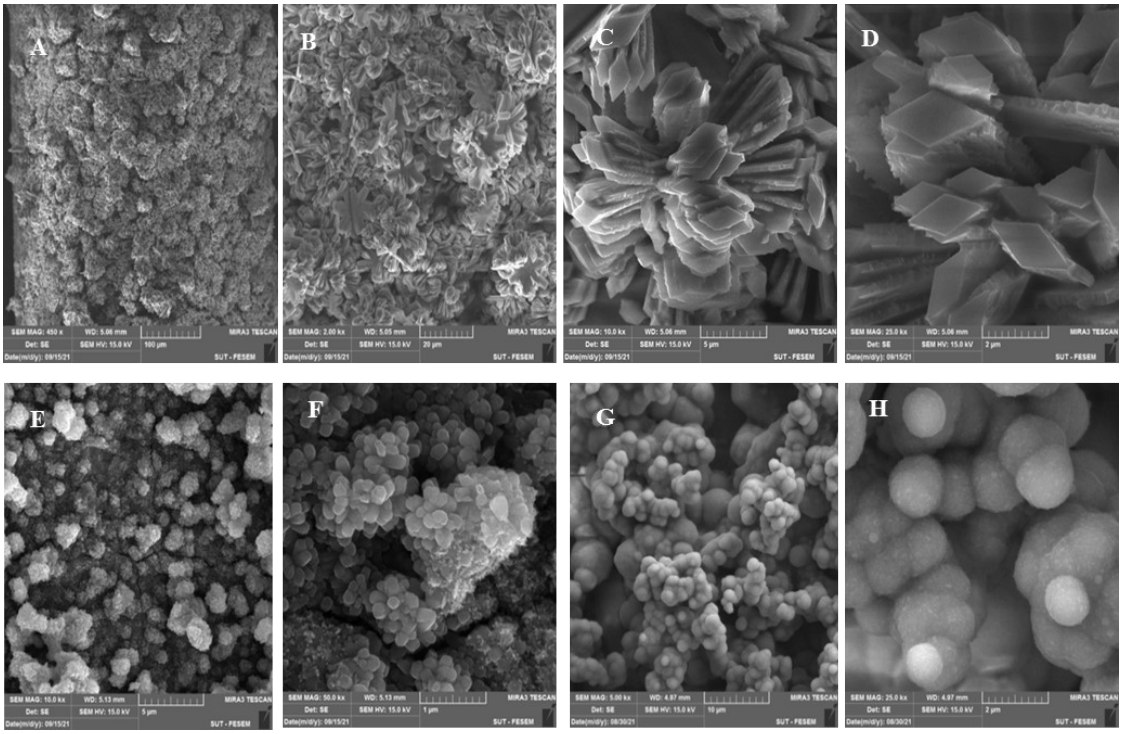

Fig. S1. FE-SEM images of rhombus- like CoV10@CW (A-D), CoV01@CW nanocube (E, F) and CoV11@CW microspheres (G, H) with different magnifications

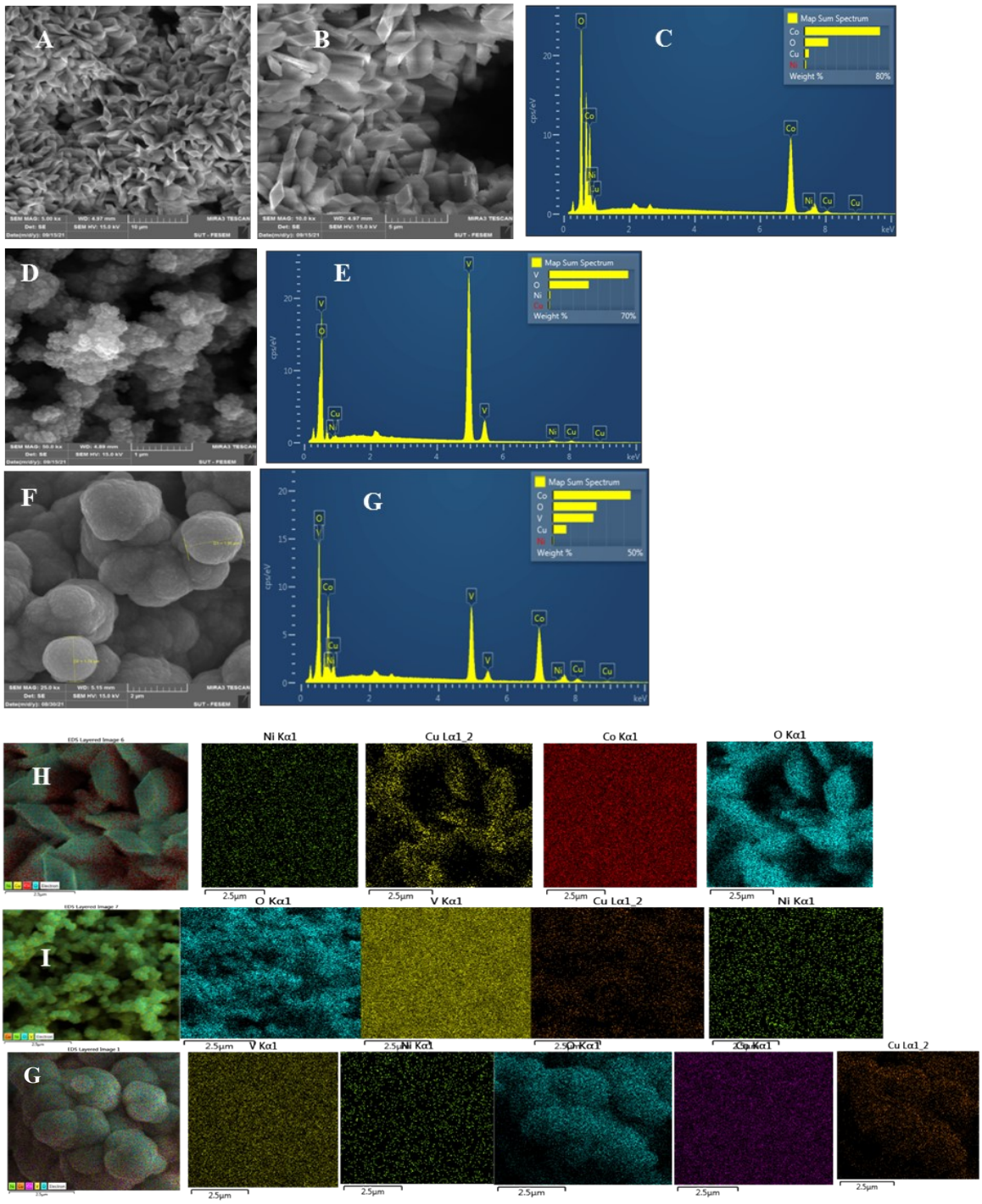

Fig. S2. FE-SEM images of rhombus- like CoV10/NiCu@CW with different magnifications (A and B), EDX spectra of rhombus- like CoV10/NiCu@CW (C), FE-SEM image (D) and EDX spectra (G) of CoV01/NiCu@CW nanocube, FE-SEM image (F) and EDX spectra (G) of CoVLDH/NiCu@CW microsphere, mapping images of rhombus- like CoV10/NiCu@CW (H), CoV01/NiCu@CW nanocube (I), and CoVLDH/NiCu@CW microsphere (J).

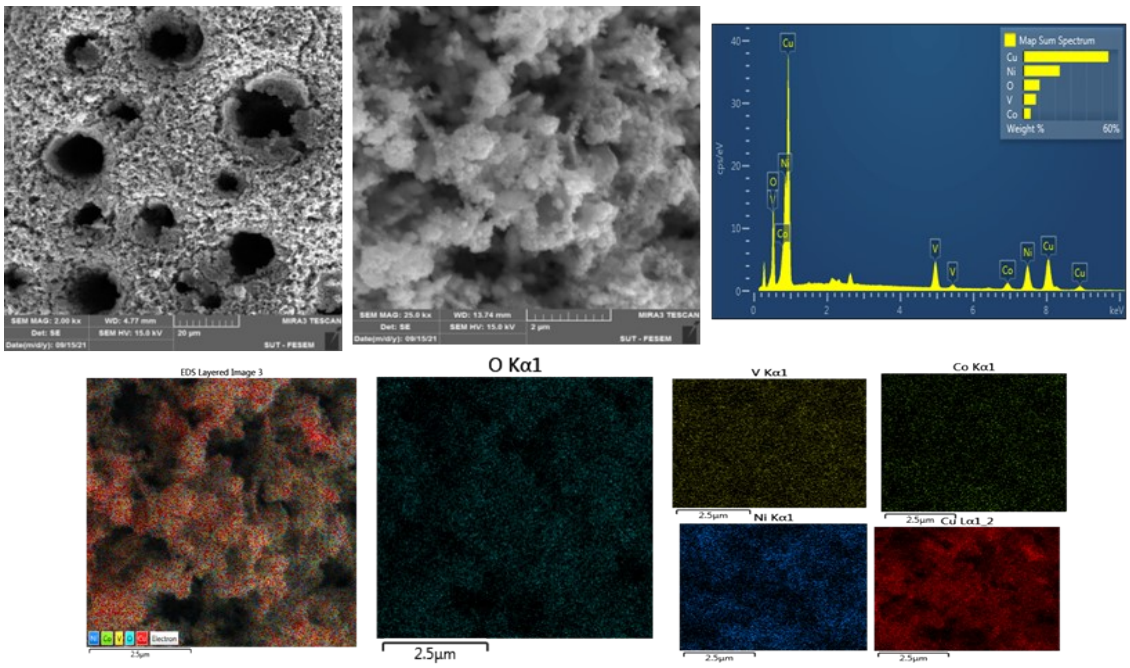

Fig. S3. FE-SEM images of e-CoV LDH/NiCu@CW with different magnifications, EDX spectra and mapping images.

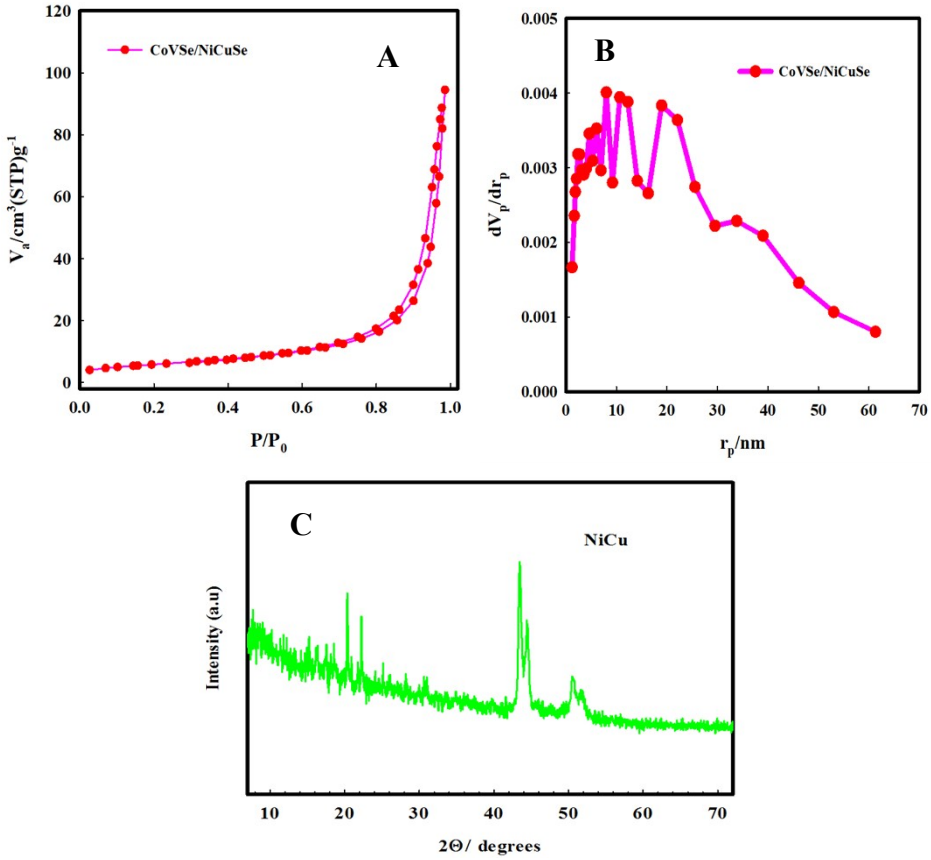

Fig. S4. (A) N_2 adsorption–desorption isotherm of the CoVSe/NiCuSe, (B) the related pore size distribution and (c) XRD spectra of NiCu

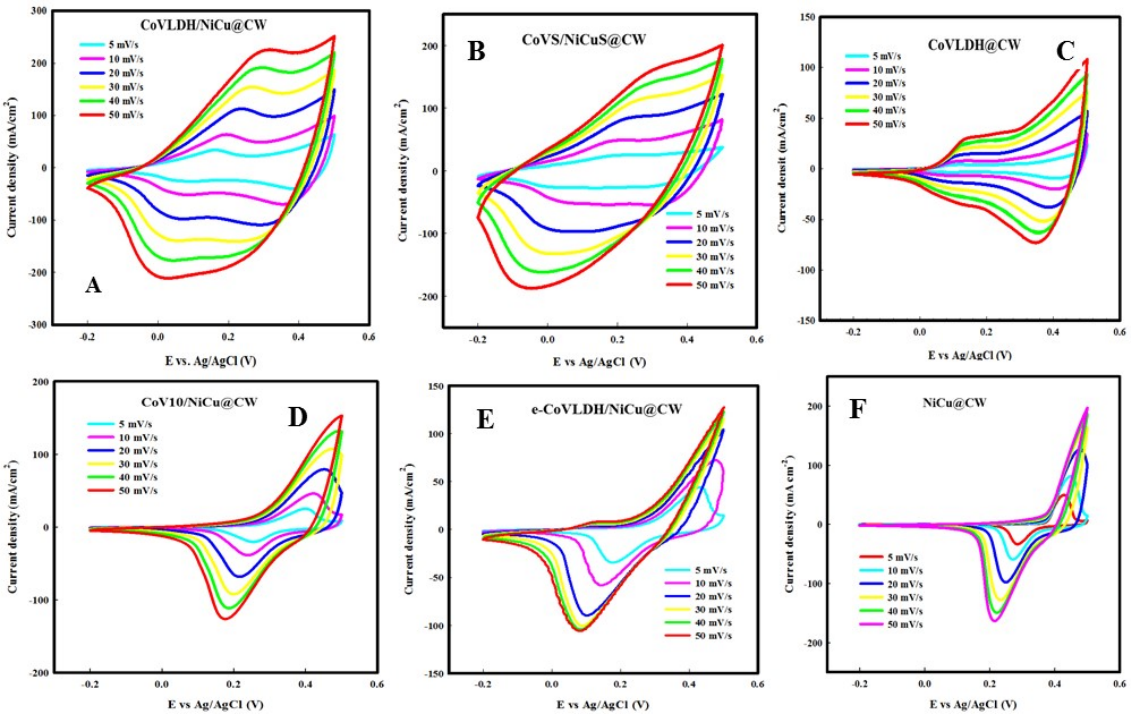

Fig. S5. CV curves of prepared fiber electrodes in 1M KOH electrolyte

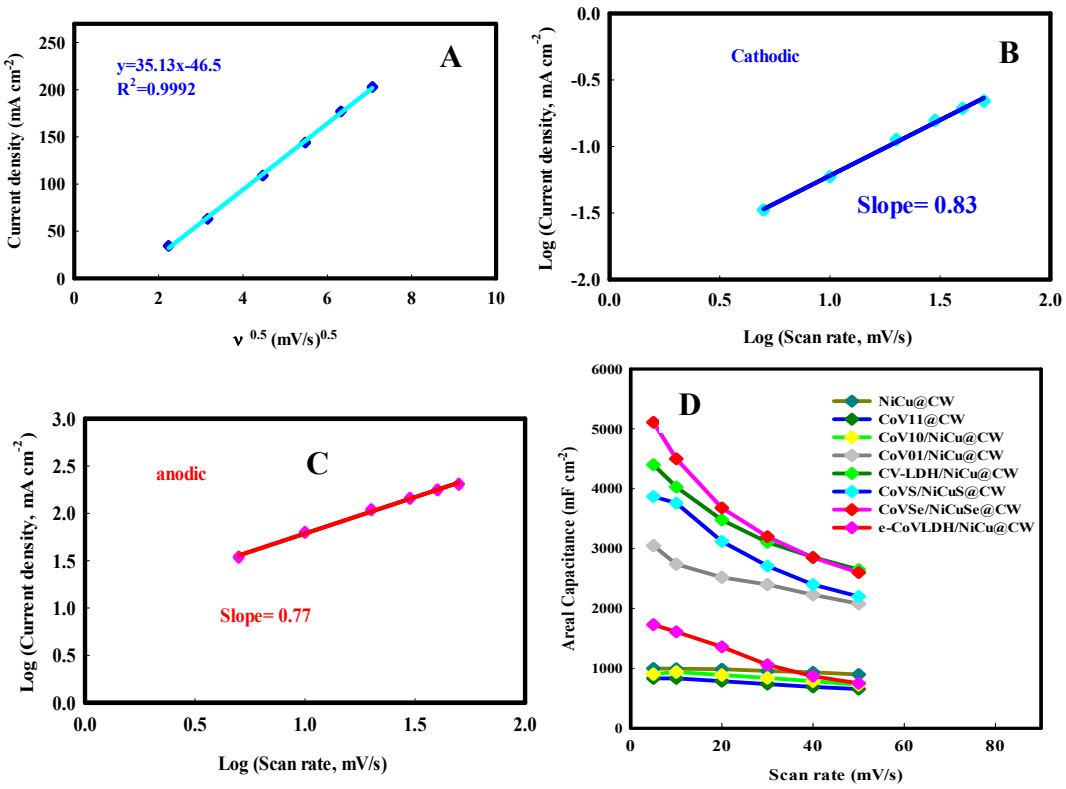

Fig. S6. (A) The peak current of CoVSe/NiCuSe@CW electrode as a function of the square root of scan rate, Logarithm relationship between the scan rate and (B) cathodic, and(C) anodic peak current. (D) Areal specific capacitance of as-prepared fiber electrodes as a function of scan rate

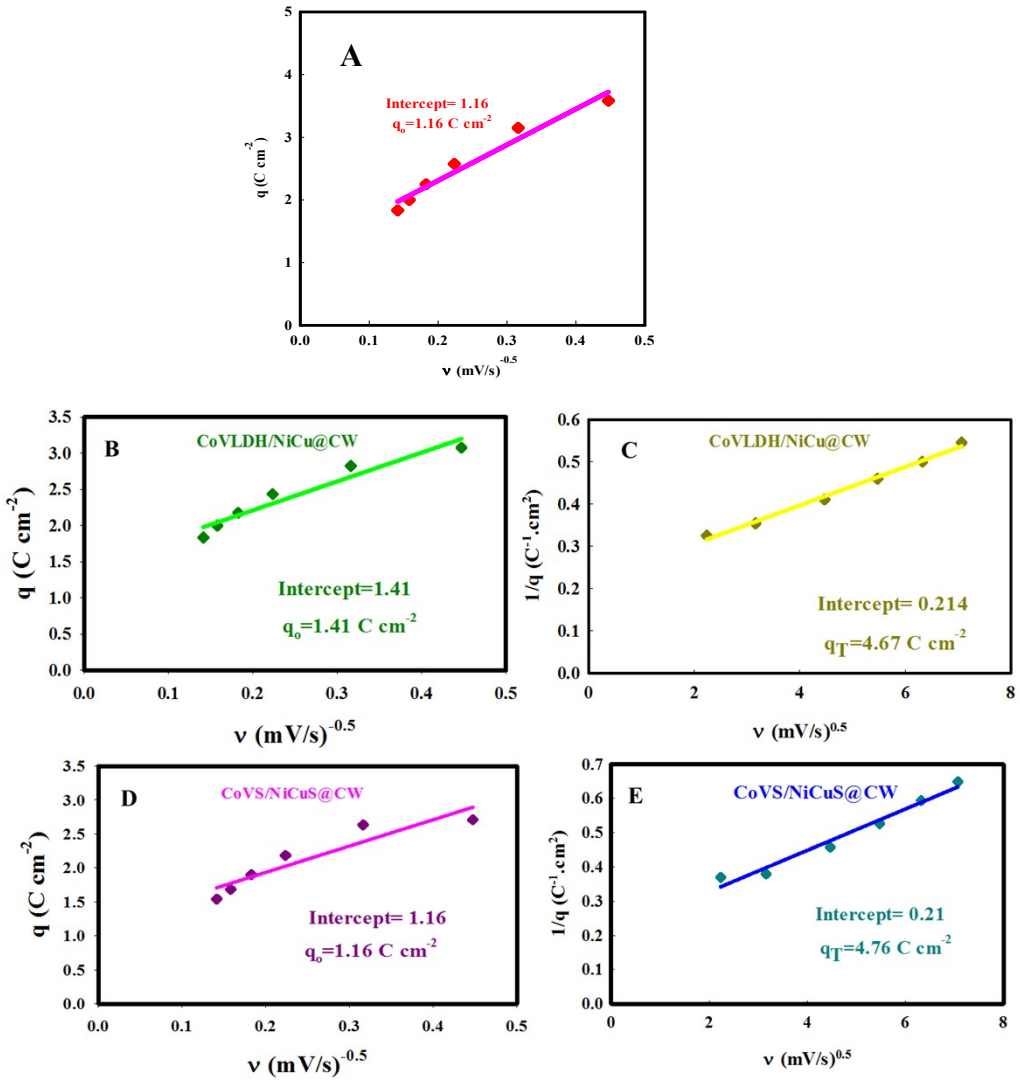

Fig. S7. Trasatti plots of q(υ) against $\upsilon^{-0.5}$ of the CoVSe/NiCuSe (A).Trasatti plots (B, D) plots of q (t) against υ-0.5, (C, E) 1/q (t) against $\upsilon^{0.5}$, for CoVLDH/NiCu@CW and CoVS/NiCuS@CW fiber electrodes

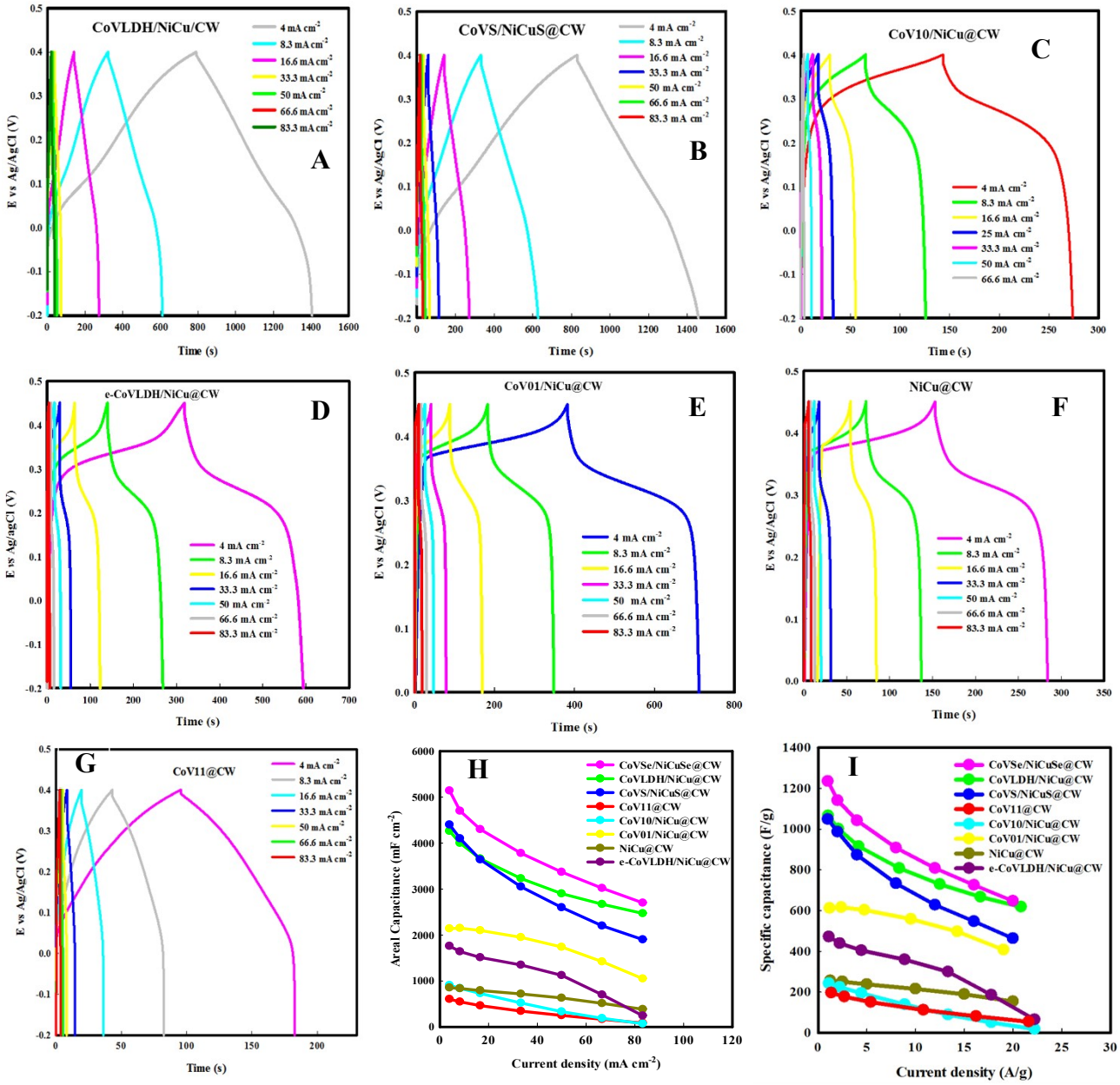

Fig. S8. GCD curves of as-prepared fiber electrodes in 1M KOH electrolyte (A-G), Areal specific capacitance of as-prepared fiber electrodes as a function of scan rate (H), Gravimetric capacitance of the different electrodes as function of current density (I)

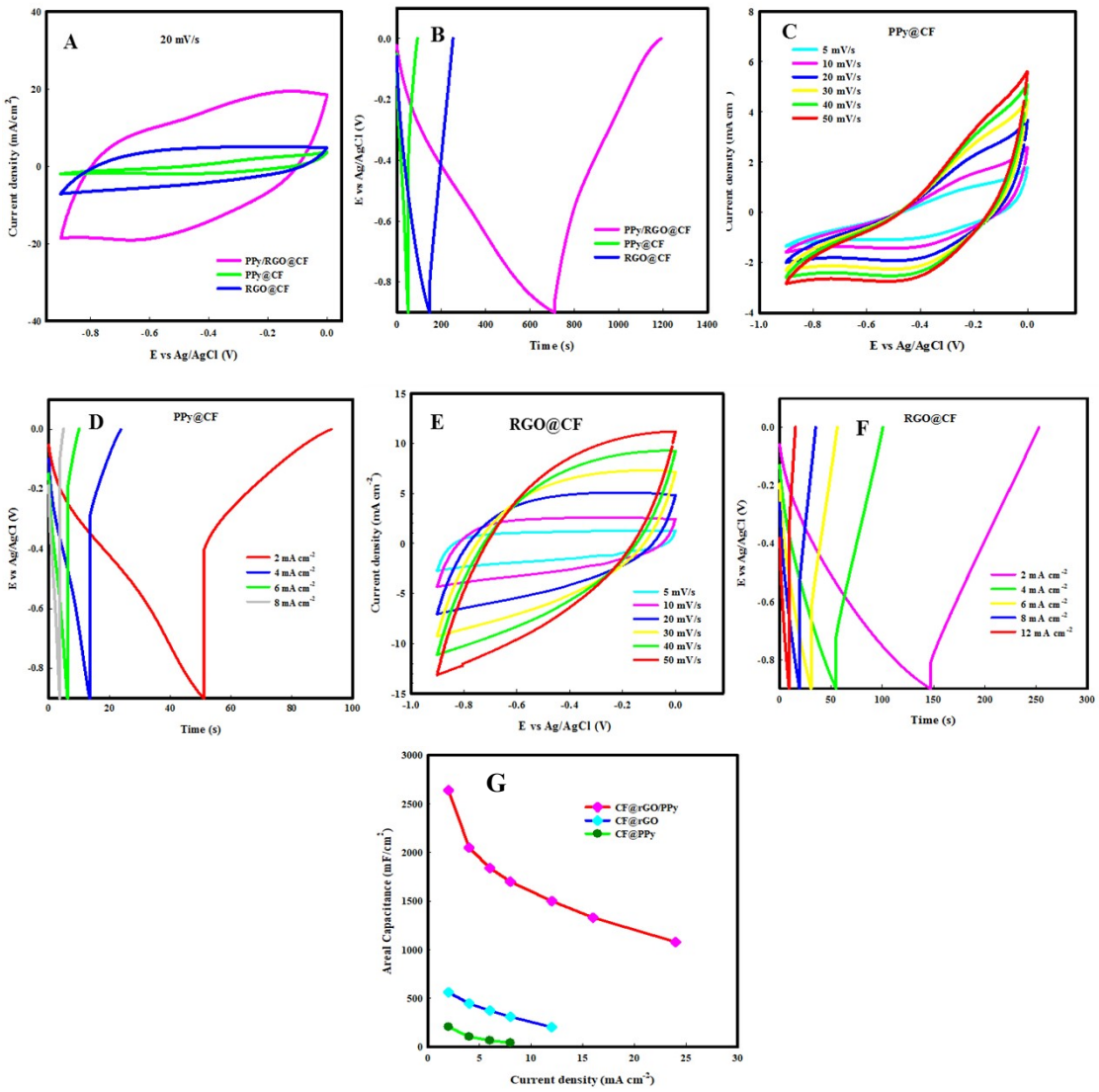

Fig. S9. Comparative CV curves of RGO@CF, PPy@CF and PPy/RGO@CF at scan rate of 20 mV/s (A), Comparative GCD curves of RGO@CF, PPy@CF and PPy/RGO@CF (B), CV curve of PPy@CF (C), GCD curve of PPy@CF (D), CV curve of RGO@CF (E) and GCD curve of RGO@CF (F) at 1M KOH electrolyte. (G) areal capacitance of RGO, PPy and PPy/RGO on the CF electrode as function of the current density.

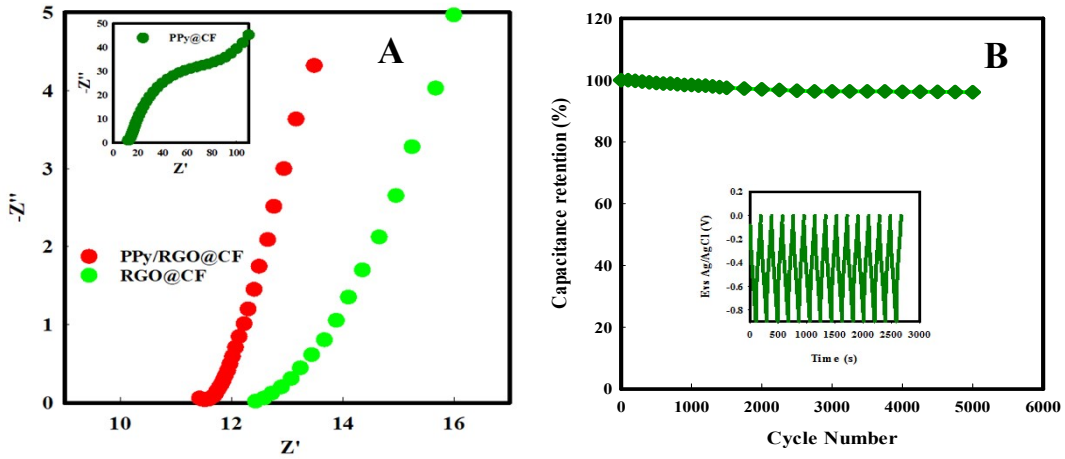

Fig. S10. The magnification of the high-frequency region (A), Cycling performance of PPy/RGO@CF (B)

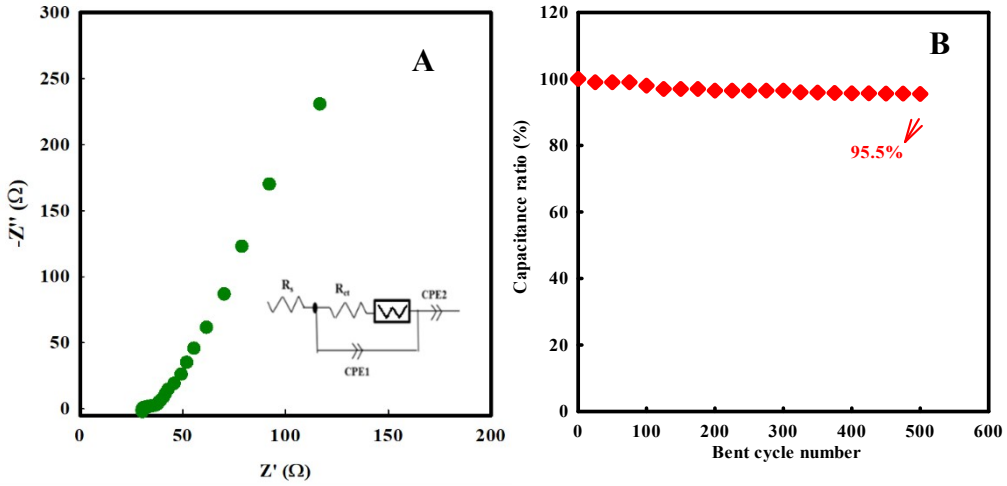

Fig. S11. Nyquist plot of the assembled all-solid-state micro- device in a frequency range of 100 kHz to 10 mHz at an open circuit potential (A), Ratio specific capacitance before and after bending of the asymmetric fiber micro-device on bent cycle number (B)

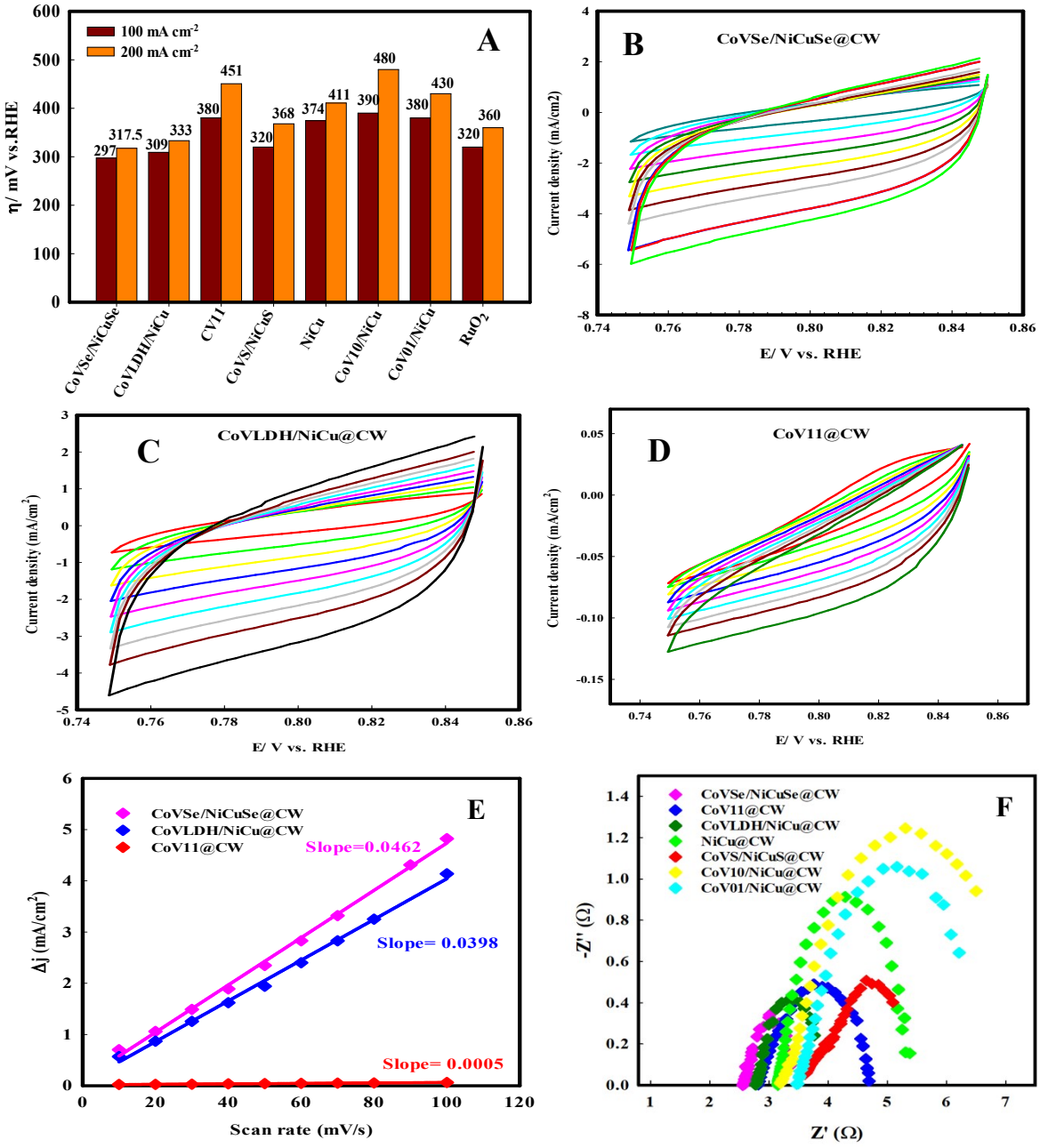

Fig. S12. Comparison of overpotentials of NiCu@CW, CoVLDH@CW, CoV01/NiCu@CW, CoV10/NiCu@CW, CoVLDH/NiCu@CW, CoVS/NiCuS@CW, CoVSe/NiCuSe@CW, and RuO2@CW obtained at a scan rate of 2 mV s-1 (A). CV curves of CoVSe/NCuSe@CW (B), CoVLDH/NiCu@CW (C) and CoV11@CW (D), in 1M KOH with different scan rates (10-100 $mV \cdot s^{-1}$). Linear fitting of the capacitive current densities of CoVLDH/NiCu@CW, CoVLDH@CW, CoVSe/NiCuSe@CW versus scan rates (E). the magnification of the high-frequency region (F).

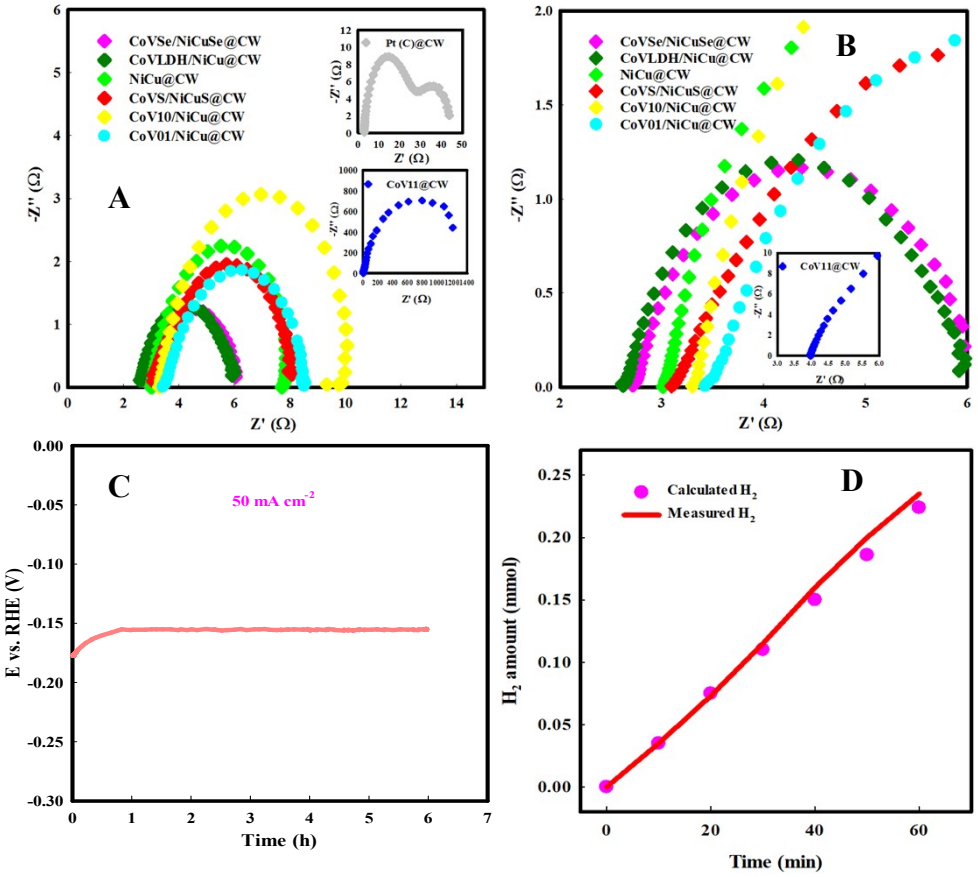

Fig. S13. EIS plots of fiber electrodes (A), the magnification of the high-frequency region (B), Time-dependent potential curve of CoVSe/NiCuSe@CW at -50 mA cm^{-2} for 6h (C), The amount of hydrogen theoretically calculated and experimentally measured *vs*. time for CoVSe/NiCuSe@CW (D).

Table S1. Comparison of specific capacitances of the present work and other electrode materials in a three-electrode system

Electrode materials	Substrate	Electroyte	Current density	Specific capacitance	Ref.
CoVSe/NiCuSe	Cu wire	1M KOH	4 mA cm^{-2}	5.14 F cm^{-2} 535.4 F cm^{-3} 617.3 mF cm^{-1}	This work
PEDOT:PSS-rGO/ MnO2	Carbon fiber	1M Na2SO4	5 mA/cm^2	2920 mF/cm2 194.25 F/cm3 549.72 mF/cm	[1]
CoVSe	Carbon cloth	2M KOH	1 mA cm^{-2}	0.327 mAh cm^{-2}	[2]
CoV-LDH	Nickel foam	1M KOH	1 A g^{-1}	1579 F g^{-1}	[3]
CNT/MnO2	carbon fiber	2M LiCl	1 A g^{-1}	277.1 F g^{-1}	[4]
MnNiCo-CH	Carbon fiber	6M KOH	1 A g^{-1}	472.23 F g^{-1}	[5]
NiVS/NiCuP	Cu wire	1M NaOH	4 mA cm^{-2}	13.4 F cm^{-2} 1.7 F cm^{-1} 1342.28 F cm^{-3}	[6]
$MnCo_2O_4$/porous Ni/Ni	Cu wire	2M KOH	2 mA cm^{-2}	1.798F cm^{-2}	[7]
CuO@CoFe-LDH	Cu wire	1M KOH	2.5 mA cm^{-2}	866 mF cm^{-2}	[8]
3D-NiCoO4	Ni wire	2M KOH	2.5 mA	38.84F cm-3	[9]
3D-NiCo2S4	Ni wire	2M KOH	0.2 mA cm^{-1}	199.74F cm^{-3} 98 mF cm^{-1} 1.248 F cm^{-2}	[10]
PPy-MnO2	Carbon fiber	4 M LiCl	50 mA cm^{-2}	3.95 F cm^{-2}	[11]

Table S2. Electrochemical properties of recent reported flexible fiber -based supercapacitors

Supercapacitor	Electrolyte	Voltage window	Capacitance	Energy density	Power density	Stability	Ref
CoVSe/NiCuSe@CW//PPy/RGO@CF	PVA-KOH	1.6 V	351.7 mF cm^{-2} 56.73 F cm^{-3}	111.4 µWh cm^{-2} 20.17 mWh cm^{-3}	12900 µW cm^{-2} 2081.14 mW cm^{-3}	96.7% after 5000 cycles	**This work**
$CoNi_2S_4$/E–NZP //rGO (solid state)	PVA-NaOH	1.8 V	241 mF cm^{-2} 18.54 F cm^{-3}	108.4 µWh cm^{-2} 8.34 mWh cm^{-3}	9280 µW cm^{-2} 716.9 mW cm^{-3}	88.89% after 5000 cycles	[12]
symmetric Cu@Ni/porous Ni/ $MnCo_2O_4$	PVA-KOH	1.3 V	54.8 mF cm^{-2} –	4.8 µWh cm^{-2}	1040 µW cm^{-2}	93.7% after 5000 cycles	[13]
$NiCo_2S_4$ //N-rGO	PVA–KOH	1 V	120 mF cm^{-2} 19.57 F cm^{-3}	32.67 µWh cm^{-2} 5.33 mWh cm^{-3}	5352.92 µW cm^{-2} 855.69 mW cm^{-3}	100 % after 5000 cycles	[14]
MnO_2/MGr/Ni	6 M KOH	0.8 V	73.2 mF cm^{-2} 9.8 F cm^{-3}	0.88 mWh cm^{-3}	25 mW cm^{-3}	no visible capacitance loss after 5000 cycles	[15]
Symmetric pErGO@Cuf/Cu wire	PVA/H_3PO_4		283.5 mF cm^{-2} –	39.3 µWh cm^{-2}	17.6 µW cm^{-2}	94.5% after 5000 cycles	[16]
VN NWAs/ CNTFs//Co_3O_4 NWAs/CNTF	KOH-PVA	1.6 V	44.4 F cm^{-3}	15.79 mWh cm^{-3}	3260 mW cm^{-3}	less than 6.88% capacitance loss after 4000 cycles	[17]
$NiCo_2O_4$@ $Ni(OH)_2$/CNTF// VN/CNTF	KOH/PVA	1.6 V	291.9 mF cm^{-2} 106.1 F cm^{-3}	103.8 µWh cm^{-2}	0.8 mW cm^{-2}	87.2% after 5000 cycles	[18]
Ni/NiO/$Ni(OH)_2$/PEDOT//Ni/CMK-3	PVA/KOH	1.45 V	31.6 mF cm^{-2} 3.16 F cm^{-3}	11 µWh cm^{-2}	7800 µW cm^{-2}	slight fluctuation for 1400 cycles	[19]
MnO_2/RGO/CF// GH/CW	PAAK/KCl	1.6 V	50.8 mF cm^{-2} 2.54 F cm^{-3}	18.1 µWh cm^{-2} 0.9 mWh cm^{-3}	200 mW cm^{-3}	90% after 10000 cycles	[20]
$Ni(OH)_2$ RGO/Ni //RGO/Ni	PVA/KOH	1.6 V	– 2.32 F cm^{-3}	0.83 mWh cm^{-3}	3430 mW cm^{-3}	~83% after 6000 cycles	[21]
Symmetric $NiCo_2O_4$/ Ni fiber	PVA–KOH	1 V		0.21 mWh cm^{-3}	15.5 mW cm^{-3}	100% after 5000 cycles	[22]
Ni_3S_2/Ni wire// Pen ink electrode	PVA/KOH	1.4 V	34.3 F g−1 87.25 mF cm−1	8.2 Wh kg^{-1} 0.81 mWh cm^{-3}	2.9 kW kg^{-1} 285 mW cm^{-3}	93.1% after 5000 cycles	[23]
Symmetric AT-PEDOT:PSS/PPy	PVA/H2SO4	0.8 V	770.6 mF cm^{-2} 393.8 F cm^{-3}	16.2 µWh cm^{-2} 8.3 mWh cm^{-3}	At 761.5 µW cm^{-2} 389.1 mW cm^{-3}	71.4% after 10000 cycles	[24]
NPG@MnO_2// CNT/Carbon paper	LiCl/PVA	1.8 V	12 mF cm^{-2} –	5.4 µWh cm^{-2}	2531 µW cm^{-2}	90% after 2000 cycles	[25]
Ni–Co DHs/nickel/pen ink/CF	PVA-KOH	1.55 V	28.67 mF cm^{-2}	9.57 µWh cm^{-2}	1841.1 µW cm^{-2}	86% after 5000 cycles	[26]
NC/VG@CNTF//VG@CNTF	PVA-KOH	1.80 V	188 F g^{-1}	90.0 Wh kg^{-1}	100 kW kg^{-1}		[27]
Ni/$Ni(OH)_2$ //Ni/OMC	PVA-KOH	1.5 V	35.67 mF cm^{-2} –	10 µWh cm^{-2} 2.16 mWh cm^{-3}	7300 µW cm^{-2} 1600 mW cm^{-3}	70% after 10 000 cycles	[28]
N- GQD/GH/CF// GH/CF	PVA/H2SO4	2 V	6.6 F cm^{-3}	3.6 mW h cm^{-3}	355.6 mW cm^{-3}	81.1% after 6000 cycles	[29]
NiCo LDH@GSs@CF–NF//AC	PVA-KOH	1.5 V	350.9 mF cm^{-2} 1.949 F cm^{-3}	109.6 µWh cm^{-2} 0.61 mWh cm^{-3}	14997.6 µW cm^{-2}	90.5% after 3000 cycles	[30]

Table S3. Comparison of OER activity with some non-noble metal based OER electrocatalysts.

Catalyst	Substrate	Electrolyte	Current density ($mA\ cm^{-2}$)	Ƞ (mV)	Tafel Slope ($mV.\ dec^{-1}$)	Ref
CoVSe/NiCuSe	Cu Wire	1.0 M KOH	100 200 600	297 317 350	67	**This work**
$CoSe_2$ microspheres	GCE	1.0 M KOH	10	330	79	[31]
$CoSe_2$ ultrathin nanosheets	CFC	1.0 M KOH	10	320	44	[32]
$CoSe_{0.85}$ **$(Ni,Co)Se_{0.85}$** **$(Ni,Co)Se_{0.85}$–NiCo LDH**	CFC CFC CFC	1.0 M KOH	10 10 10	324 216 255	85 79 77	[33]
$CoSe_2$@C-CNT	Carbon Cloth	1.0 M KOH	10 50	306 345	46	[34]
$CoSe_2$@N/C-CNT	GCE	1.0 M KOH	10	340	107	[35]
ZIF-$Co_{0.85}Se$	GCE	1.0 M KOH	10	360	62	[36]
CoO/$CoSe_2$	Ti mesh	PBS	10	510	137	[37]
Zn-doped $CoSe_2$	carbon fabric collector (CFC)	1.0 M KOH	10	356	88	[38]

Reference:

[1] L. Naderi, S. Shahrokhian, F. Soavi, *J. Mater. Chem. A*, 2020, **8**, 19588-19602.

[2] A. K. Das, B. Ramulu, E. G. Shankar, J. S. Yu, *Chem. Eng. J*., 2022, **429**, 132486

[3] S. C. Lee, M. Kim, J.H. Park, E. S. Kim, Sh. Liu, K. Y. Chung, S. Ch. Jun, *J. Power Sources*, 2021, **486**, 229341.

[4] T. Cenab, L.Chena, X. Zhang, Y. Tian, X. Fan, *Electrochim. Acta*, 2021, **367**, 137488

[5] X. Cao, Y. Liu, Y. Zhong, L. Cui, A. Zhang, J. M. Razal, W. Yang, J. Liu, *J. Mater. Chem. A*, 2020, **8**, 1837-1848.

[6] L. Naderi, S. Shahrokhian, *Chem. Eng. J*., 2020, **392**, 124880.

[7] Y. Ji, J. Xie, J. Wu, Y. Yang, X.Z. Fua, R. Sun, C.P. Wong, *J. Power Sources*, 2018, **393** 54–61.

[8] Z. Li, M. Shaon, L. Zhou, R. Zhang, C. Zhang, J. Han, M. Wein, D.G. Evans, X. Duan, *Nano Energy*, 2016, **20**, 294–304.

[9] A. Ramadoss, K.-N. Kang, H.-J. Ahn, S.-I. Kim, S.-T. Ryu, J.-H. Jang, *J. Mater. Chem. A*, 2016, **4**, 4718–4727.

[10] B. Saravanakumar, S.S. Jayaseelan, M.K. Seo, H.Y. Kim, B.S. Kim, *Nanoscale*, 2017, **9**, 18819-18834.

[11] W. Liu, N. Liu, Y. Shi, Y. Chen, C. Yang, J. Tao, S. Wang, Y. Wang, J. Su, L. Li, Y. Gao. *J. Mater. Chem. A*, 2015, **3**, 13461-13467.

[12] S. Shahrokhian, L. Naderi, *J. Phys. Chem. C,* 2019, **123**, 21353–21366.

[13] Y. Ji, J. Xie, J. Wu, Y. Yang, X.Z. Fu, R. Sun, C.P. Wong, *J. Power Sources* 2018, **393**, 54–61.

[14] B. Saravanakumar, S.S. Jayaseelan, M.K. Seo, H.Y. Kim, B.S. Kim, *Nanoscale,* 2017, **9** 18819–18834.

[15] M. Hu, Y. Liu, M. Zhang, H. Wei, Y. Gao, *J. Power Sources,* 2016, **335**, 113–120.

[16] T. Purkait, G. Singh, D. Kumar, M. Singh, R.S. Dey, Sci. Rep., 2018, **8**, 640–653.

[17] J. Sun, P. Man, Q. Zhang, B. He, Zh. Zhou, Ch. Li, X. Wang, J. Guo, J. Zhao, L. Xie, Q. Li, J. Sun, G. Hong, Y. Yao, *Appl. Surf. Sci*., 2018, **447**, 795–801.

[18] X. Wang, J. Sun, J. Zhao, Zh. Zhou, Q. Zhang, Ch. Wong, Y. Yao., *J. Phys. Chem. C,* 2019, **123**, 985-993.

[19] H. Yang, H. Xu, M. Li, L. Zhang, Y. Huang, X. Hu, *ACS Appl. Mater. Interfaces,* 2016, **8**, 1774–1779.

[20] Z. Zhang, F. Xiao, S. Wang, *J. Mater. Chem. A,* 2015, **3**, 11215–11223.

[21] K. Lu, J. Zhang, Y. Wang, J. Ma, B. Song, H. Ma, *ACS Sustainable Chem. Eng.,* 2017, **5**, 821–827.

[22] A. Ramadoss, K.N. Kang, H.J. Ahn, S.I. Kim, S.T. Ryu, J.H. Jang, *J. Mater. Chem. A,* 2016, **4**, 4718–4727.

[23] J. Wen, S. Li, K. Zhou, Z. Song, B. Li, Z. Chen, T. Chen, Y. Guo, G. Fang, *J. Power Sources,* 2016, **324**, 325–333.

[24] W. Teng, Q. Zhou, X. Wang, H. Che. P. Hu, H. Li, J. Wang. *Chem. Eng. J.,* 2020, **390**, 124569.

[25] H. Xu, X. Hu, Y. Sun, H. Yang, X. Liu, Y. Huang, *Nano Res*., 2015, **8**, 1148–1158.

[26] L. Gao, J. U. Surjadi, K. Cao, H. Zhang, P. Li, Sh. Xu, Ch. Jiang, J. Song, D. Sun, Y. Lu, *ACS Appl. Mater. Interfaces,* 2017, **9**, 5409−5418

[27] J. G. Kim, H. Yu, J.Y. Jung, M. J. Kim, D. Y. Jeon, H. S. Jeong, N. D. Kim, *Adv. Funct. Mater.,* 2022, 2113057.

[28] X. Dong, Z. Guo, Y. Song, M. Hou, J. Wang, Y. Wang, Y. Xia, *Adv. Funct. Mater.,* 2014, **24**, 3405–3412.

[29] Z. Li, J. Wei, J. Ren, X. Wua, L. Wang, D. Pan, M. Wu, *Carbon,* 2019, **154**, 410-419.

[30] L. Gao, J. Song, J. U. Surjadi, K. Cao,Y. Han, D. Sun, X. Tao, Y. Lu., *ACS Appl. Mater. Interfaces,* 2018, **10**, 28597-28607.

[31] X. Liu , Y. Liu, L. Z. Fan, *J. Mater. Chem. A*, 2017, **5**, 15310-15314.

[32] Y. Liu, H. Cheng, M. Lyu, S. Fan, Q. Liu, W. Zhang, Y. Zhi, C. Wang, C. Xiao, S. Wei, B. Ye and Y. Xie, *J. Am. Chem. Soc.,* 2014, **136**, 15670–15675.

[33] Ch. Xia , Q. Jiang , Ch. Zhao , M. N. Hedhili , H. N. Alshareef, *Adv. Mater.,* 2016, **28**, 77–85.

[34] M. Yuan, M. Wang, P. Lu, Y. Sun, S. Dipazir, J. Zhang, S. Li, G. Zhang, *J. Colloid Interface Sci.,* 2019, **533**, 503-512.

[35] H. Ding, G. Xu, L. Zhang, B. Wei, J. Hei, L. Chen, *J. Colloid Interface Sci.,* 2020, **566**, 296-303.

[36] S. Li, S. Peng, L. Huang, X. Cui, A. M. Al-Enizi, G. Zheng, *ACS Appl. Mater. Interfaces,* 2016, **8**, 20534–20539.

[37] K. Li, J. Zhang, R. Wu, Y. Yu, B. Zhang, *Adv. Sci.,* 2016, **3**, 1500426.

[38] Q. Dong, Q. Wang, Z. Dai, H. Qiu, X. Dong, *ACS Appl. Mater. Interfaces,* 2016, **8**, 26902–26907.